EARTHQUAKE ENGINEERING AND STRUCTURAL DYNAMICS
Earthquake Engng Struct. Dyn. 2000; **29**: 711–729

Flexibility of superstructures and supports in the seismic analysis of simple bridges

Farid Alfawakhiri[1,*,†] and Michel Bruneau[2]

[1] *Canadian Steel Construction Council, 300-201 Consumers Rd., Willowdale, ON, Canada M2J 4G8*
[2] *Multidisciplinary Centre for Earthquake Engineering Research, State University of New York at Buffalo, Buffalo, NY 14261-0025, U.S.A*

SUMMARY

This paper addresses the elastic dynamic response of simply supported bridges to ground motion in their transverse direction. The interaction between superstructure and support flexibilities is studied in a systematic manner for symmetric spans. The bridges are modelled as beams with uniformly distributed mass and elasticity, simply supported at the ends by elastic springs. It is shown that a dimensionless stiffness index, which reflects the relative stiffness of the superstructure compared to the stiffness of the substructure, completely defines the dynamic mode shapes of the model. Useful closed-form expressions, based on approximate shape functions, are derived for the dynamic parameters of the first mode, and their accuracy is assessed. The effect of the stiffness index on these dynamic parameters is investigated. Numerical case studies are presented to illustrate the use of proposed equations in the seismic analysis of bridges. Copyright © 2000 John Wiley & Sons, Ltd.

KEY WORDS: seismic loads; analysis; bridges; flexible superstructure; mode shapes; modelling

INTRODUCTION

The structural analysis of bridges for earthquake loads often employs simplifying assumptions of infinitely rigid superstructure or translationally rigid supports. While the infinite rigidity cannot be achieved in practice, such assumptions are justified in many instances. However, there is little (if any) guidance provided in the literature with regard to how unaccounted flexibilities affect the dynamic response of bridges and when such effects become significant. In other words, it is not always clear, how stiff the structure should be in order to justify the assumption of infinite rigidity.

Considerable flexibility of a bridge superstructure in the horizontal transverse direction may be encountered in relatively narrow (slender in plan view) bridges. Support (substructure) flexibility, commonly attributed to piers, also includes, in a broader sense, flexibility of bearings and end diaphragms of slab-on-girder [1] or deck-truss [2] steel bridges. This paper addresses the interaction between these superstructure and support flexibilities of bridge systems in the

* Correspondence to: Farid Alfawakhiri, M-59, FRM, Institute for Research in Construction, National Research Council of Canada, Montreal Road, Ottawa, Ontario K1A 0R6, Canada.
† E-mail: farid.alfawakhiri@nrc.ca

Received 27 May 1999
Accepted 16 November 1999

perspective of quantifying the errors arising when simplifying approximations of infinite rigidity are made, and the instances where these errors become significant. Elastic response of symmetric simply supported bridges to transverse ground motion is studied in this context. In this study, bridges are modelled as beams with uniformly distributed mass and stiffness, simply supported at the ends by elastic springs. The inertial moment associated with rotation of beam sections and deflections due to shear stress in the beam are neglected.

NATURAL VIBRATION FREQUENCIES AND MODES

Consider the beam shown in Figure 1, having a uniform mass $m(x) = m = M/L$ (where M is the total mass of the beam) and a uniform stiffness $\mathrm{EI}(x) = \mathrm{EI}$. The beam is supported at the ends by two linear springs of stiffness K_e acting in the beam's transverse direction, while the beam ends are free to rotate, but completely restricted from translation in the beam's longitudinal direction. The dynamic transverse undamped free vibration response of such a uniform straight beam [3] is

$$u(x, t) = \varphi(x) z(t) \tag{1}$$

where the transverse displacement of the beam, u, varies with both time, t, and position, x, along the beam. The time function $z(t)$ and the spatial function $\varphi(x)$ can be, respectively, obtained by solving

$$\ddot{z}(t) + \omega^2 z(t) = 0 \tag{2}$$

and

$$\mathrm{EI}\,\varphi^{\mathrm{iv}}(x) - \omega^2 m\,\varphi(x) = 0 \quad \text{or} \quad \varphi^{\mathrm{iv}}(x) - \beta^4 \varphi(x) = 0 \tag{3}$$

where

$$\beta^4 = \frac{\omega^2 m}{\mathrm{EI}} \tag{4}$$

The general solution of Equation (3) has the form

$$\varphi(x) = C_1 \sin \beta x + C_2 \cos \beta x + C_3 \sinh \beta x + C_4 \cosh \beta x \tag{5}$$

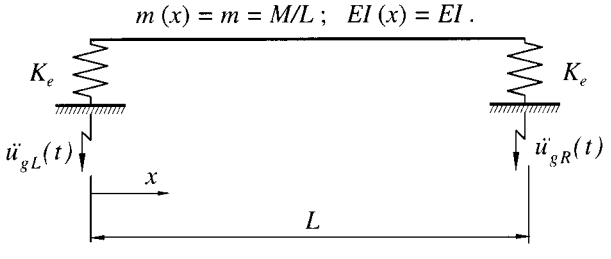

Figure 1. Uniform beam simply supported on elastic springs.

containing four unknown constants C_1, C_2, C_3, C_4 and the unknown eigenvalue parameter β defined by Equation (4). The introduction of the four boundary conditions at the ends of the beam will give four simultaneous equations, which can be solved for β_n (i.e. for the natural frequencies ω_n) and for three constants in terms of the fourth, resulting in the natural mode shapes $\varphi_n(x)$ of Equation (5). For the considered beam, due to the symmetry about an axis parallel to the springs and passing through the midspan, two sets of boundary conditions (and hence, two associated groups of mode shapes) can be recognized, namely, symmetric and antisymmetric. The bending moments at beam ends are always equal to zero, while the displacements of the ends are equal in magnitude and proportional to the shear force. In the symmetric set of boundary conditions the displacements of the beam ends have the same direction, and the antisymmetric boundary conditions suggest that the ends are displaced in two opposite directions.

First, consider the symmetric boundary conditions. At $x = 0$

$$\mathscr{M}(0) = 0 \Rightarrow \mathrm{EI}\,\varphi''(0) = 0 \Rightarrow -C_2 + C_4 = 0 \tag{6}$$

$$u(0) = -V(0)/K_e \Rightarrow \varphi(0) = -\mathrm{EI}\,\varphi'''(0)/K_e \Rightarrow C_2 + C_4 = \frac{\beta^3\,\mathrm{EI}}{K_e}(C_1 - C_3) \tag{7}$$

These two equations give

$$C_2 = C_4 = 0.5B(\beta L)^3\,(C_1 - C_3) \tag{8}$$

where

$$B = \frac{\mathrm{EI}}{K_e L^3} \tag{9}$$

Then, using Equations (5), (8) and (9), at $x = L$

$$\mathscr{M}(L) = 0 \Rightarrow \mathrm{EI}\,\varphi''(L) = 0 \Rightarrow -C_1 \sin\beta L + 0.5B(\beta L)^3\,(C_1 - C_3)\,(\cosh\beta L - \cos\beta L) + C_3 \sinh\beta L = 0 \tag{10a}$$

$$u(L) = -V(0)/K_e \Rightarrow \varphi(L) = -\mathrm{EI}\,\varphi'''(0)/K_e \Rightarrow C_1 \sin\beta L + 0.5B(\beta L)^3(C_1 - C_3) \times (\cosh\beta L + \cos\beta L) + C_3 \sinh\beta L = B(\beta L)^3(C_1 - C_3) \tag{10b}$$

Subtracting Equation (10a) from Equation (10b), gives

$$2C_1 \sin\beta L + B(\beta L)^3(C_1 - C_3)\cos\beta L = B(\beta L)^3(C_1 - C_3)$$

which, knowing that $\sin\beta L/(\cos\beta L - 1) = \cot(\beta L/2)$, simplifies to

$$C_3 = \left(1 - \frac{2\cot 0.5\,\beta L}{B(\beta L)^3}\right) C_1 \tag{11a}$$

For antisymmetric mode shapes, using the antisymmetric boundary condition $u(L) = V(0)/K_e$, and knowing that $\sin \beta L/(\cos \beta L + 1) = \tan(\beta L/2)$, a similar derivation gives

$$C_3 = \left(1 + \frac{2 \tan 0.5\beta L}{B(\beta L)^3}\right) C_1 \tag{11b}$$

Further, denoting the association with symmetric and antisymmetric modes by subscripts s and a, respectively, and using Equations (8) and (11), the mode shape Equation (5) can be reformulated for symmetric and antisymmetric mode shapes as follows:

$$\varphi_s(x) = C_1\left[\sin \beta_s x + \sinh \beta_s x + \cot 0.5\, \beta_s L\left(\cos \beta_s x + \cosh \beta_s x - \frac{2 \sinh \beta_s x}{B(\beta_s L)^3}\right)\right] \tag{12a}$$

$$\varphi_a(x) = C_1\left[\sin \beta_a x + \sinh \beta_a x - \tan 0.5\, \beta_a L\left(\cos \beta_a x + \cosh \beta_a x - \frac{2 \sinh \beta_a x}{B(\beta_a L)^3}\right)\right] \tag{12b}$$

The value of C_1 is arbitrary. In a particular numerical case, for every $\varphi_n(x)$, it is useful to choose C_1 so that the maximum value of $\varphi_n(x)$ is equal to unity. The values of β_s and β_a can be determined from the boundary condition $\varphi''(L) = 0$ as follows.

For symmetric mode shapes, at $x = L$

$$C_1 L^2\left[-\sin \beta_s L + \sinh \beta_s L + \cot 0.5 \beta_s L\left(-\cos \beta_s L + \cosh \beta_s L - \frac{2 \sinh \beta_s L}{B(\beta_s L)^3}\right)\right] = 0 \tag{13}$$

Non-trivial solution of Equation (13) requires C_1 to have a non-zero value. Further, multiplying Equation (13) by $B\,(\beta_s L)^3$ and dividing it by $C_1 L^2 (\cosh \beta_s L - 1)$, gives the frequency equation

$$B(\beta_s L)^3 (\cot\, 0.5\, \beta_s L + \coth\, 0.5 \beta_s L) - 2 \cot 0.5 \beta_s L \coth\, 0.5 \beta_s L = 0 \tag{14a}$$

A similar derivation produces the frequency equation for antisymmetric mode shapes

$$B(\beta_a L)^3 (\tan 0.5 \beta_a L - \tanh 0.5 \beta_a L) - 2 \tan 0.5 \beta_a L \tanh 0.5 \beta_a L = 0 \tag{14b}$$

No simple closed-form solution is available for $\beta_n L$ (subscript n denotes the association with any mode, symmetric or antisymmetric). Equations (14a) and (14b) can be solved numerically by graphical or iterative methods to obtain the values of $\beta_n L$ for any desired number of modes with any desired level of accuracy. The natural mode frequencies then can be found using Equation (4)

$$\omega_n = (\beta_n L)^2 \sqrt{\frac{\mathrm{EI}}{ML^3}} \tag{15}$$

From Equations (14) it is seen that parameters $\beta_n L$ depend only on the dimensionless stiffness index B, defined by Equation (9). It follows, that B completely defines the normalized mode shapes

$$\bar{\varphi}_s(\bar{x}) = C_1\left[\sin \alpha_s \bar{x} + \sinh \alpha_s \bar{x} + \cot 0.5\, \alpha_s\left(\cos \alpha_s \bar{x} + \cosh \alpha_s x - \frac{2 \sinh \alpha_s \bar{x}}{B\alpha_s^3}\right)\right] \tag{16a}$$

$$\bar{\varphi}_a(\bar{x}) = C_1\left[\sin \alpha_a \bar{x} + \sinh \alpha_a \bar{x} - \tan 0.5 \alpha_a\left(\cos \alpha_a \bar{x} + \cosh \alpha_a \bar{x} - \frac{2 \sinh \alpha_a \bar{x}}{B\alpha_a^3}\right)\right] \tag{16b}$$

where

$$\bar{x} = \frac{x}{L} \tag{17}$$

and

$$\alpha = \beta L \tag{18}$$

In other words, beams having the same stiffness index B will have the same infinite set of non-dimensional mode shapes defined by Equations (16).

Expressions on the left-hand side of Equations (14) are even functions of $\beta_n L$, i.e. $f(-\beta_n L) = f(\beta_n L)$. The sign of $\beta_n L$ is also of no importance in Equation (15) (because $\beta_n L$ is squared) and Equations (12) or (16) (because C_1 is arbitrary). It follows, that only the positive (or negative) range of βL needs to be investigated. Further examination of Equations (14) in the interval $0 < \beta L < \pi$ shows that, for any positive finite value of B, Equation (14a) has a single root in that interval, while Equation (14b) has none. It means that the fundamental natural vibration mode shape is symmetric. It is possible then to derive approximate expressions for the first natural vibration frequency ω_1 as follows. Rewriting Equation (13) in terms of α_s, dividing it by $C_1 L^2$ and multiplying it by $B\alpha_s^3$ $(\cos\alpha_s - 1)$, gives

$$B\alpha_s^3(\sin\alpha_s - \sinh\alpha_s + \cos\alpha_s\sinh\alpha_s - \sin\alpha_s\cosh\alpha_s) + 2\sin\alpha_s\sinh\alpha_s = 0 \tag{19}$$

Expansion of the left-hand side of Equation (19) in the form of Maclaurin's power series

$$f(\alpha_s) = f(0) + \alpha_s f'(0) + \frac{\alpha_s^2}{2!}f''(0) + \frac{\alpha_s^3}{3!}f'''(0) + \frac{\alpha_s^4}{4!}f^{iv}(0) + \cdots$$

gives

$$\frac{\alpha_s^2}{2!}(4) + \frac{\alpha_s^6}{6!}(720B + 16) + \frac{\alpha_s^{10}}{10!}(10\,080B + 64) + \frac{\alpha_s^{14}}{14!}(144\,144B + 256) + \frac{\alpha_s^{18}}{18!}(1\,243\,584\,\mathrm{B} + 1024) + \cdots = 0 \tag{20}$$

Keeping only the first three terms of the left-hand side of Equation (20) (i.e neglecting higher order terms) and dividing them by α_s^2, gives a quadratic equation in terms or α_s^4, which can be solved for the smaller root

$$\alpha_1^4 = \frac{1260}{(315B + 2)}(45B + 1 - \sqrt{2025B^2 + 45B + 5/7}) \tag{21}$$

Then, using Equations (15), (18) and (21), an approximate formula for the fundamental frequency is obtained

$$\omega_1 = \sqrt{\frac{1260\mathrm{EI}}{(315B + 2)ML^3}(45B + 1 - \sqrt{2025B^2 + 45B + 5/7})} \tag{22}$$

A simpler, but less accurate, expression for ω_1 could be obtained by also neglecting the third term (in addition to higher order terms) of the left-hand side of Equation (20). The remaining two terms

are divided by α_s^2 and the resulting linear equation is solved for α_s^4. Using Equations (15) and (18), the fundamental frequency can be expressed as

$$\omega_1 = \sqrt{\frac{90\,\mathrm{EI}}{(45B+1)\,ML^3}} \tag{23}$$

More convenient approximate expressions for the fundamental frequency could be obtained by using approximate first mode shapes, as will be discussed later.

MODAL ANALYSIS

When the eigenvalue problem of Equation (3) is solved for the natural frequencies and mode shapes, the total displacement response of the beam is given by the linear combination of the contributions of all the modes

$$u(x,t) = \sum_{n=1}^{\infty} u_n(x,t) = \sum_{n=1}^{\infty} \varphi_n(x)\, z_n(t) \tag{24}$$

The modal co-ordinates $z_n(t)$ are found from the modal equations of motion

$$M_n \ddot{z}_n(t) + K_n z_n(t) = P_n(t) \tag{25}$$

where M_n, K_n and P_n are, respectively, the generalized mass, the generalized stiffness and the generalized force, of the nth mode, for elastic systems with uniformly distributed mass and stiffness. For the considered system, in the following expanded expression for the generalized stiffness [3]:

$$K_n = \mathrm{EI}\,\varphi_{\mathrm{n}}(x)\,\varphi_{\mathrm{n}}'''(x)|_0^L - \mathrm{EI}\,\varphi_{\mathrm{n}}'(x)\,\varphi_{\mathrm{n}}''(x)|_0^L + \mathrm{EI}\int_0^L \varphi_{\mathrm{n}}''(x)\,\varphi_{\mathrm{n}}''(x)\,\mathrm{d}x \tag{26}$$

the second term of the right-hand side is equal to zero because $\varphi''(0) = 0$ and $\varphi''(L) = 0$ (the ends of the beam are free to rotate). Furthermore, knowing that for both symmetric and antisymmetric boundary conditions $\mathrm{EI}\,\varphi(L)\,\varphi'''(L) = -\mathrm{EI}\,\varphi(0)\,\varphi'''(0) = K_e[\varphi(0)]^2$, Equation (26) simplifies to

$$K_n = 2K_e[\varphi_{\mathrm{n}}(0)]^2 + \mathrm{EI}\int_0^L [\varphi_{\mathrm{n}}''(x)]^2\,\mathrm{d}x \tag{27}$$

Note that the first term of the right-hand side of Equation (27) vanishes, when $K_e = \infty$ and $\varphi_{\mathrm{n}}(0) = 0$ (as in the case of a beam with translationally rigid supports).

The expression for the generalized force [3]

$$P_n = \int_0^L p(x,t)\,\varphi_{\mathrm{n}}(x)\,\mathrm{d}x \tag{28}$$

suggests that for any antisymmetric mode shape $\varphi_{\mathrm{a}}(x)$, the modal generalized force P_n is equal to zero, if the dynamic force $p(x,t)$ is symmetric. It means, the antisymmetric modes will not contribute to the total response, unless $p(x,t)$ is non-symmetric (has an antisymmetric component). By the same logic, the symmetric modes will not respond to an antisymmetric dynamic force.

It follows, that in the general case of an arbitrary $p(x, t)$, symmetric mode shapes will respond only to the symmetric component $p_s(x, t)$ of the dynamic force, while the antisymmetric modes will respond only to its antisymmetric component $p_a(x, t)$. Then, the modal equations of motion can be separated into two groups

$$M_s\ddot{z}_s(t) + K_s z_s(t) = P_s(t) \tag{29}$$

$$M_a\ddot{z}_a(t) + K_a z_a(t) = P_a(t) \tag{30}$$

where

$$P_s = \int_0^L p_s(x, t)\,\varphi_s(x)\,\mathrm{d}x \tag{31}$$

$$P_a = \int_0^L p_a(x, t)\,\varphi_a(x)\,\mathrm{d}x \tag{32}$$

Similar approach is valid when analysing the response of the beam to earthquake induced ground motions in the transverse direction. In the general case of multiple support excitation, when the left and right supports are subjected to different ground accelerations $\ddot{u}_{gL}(t)$ and $\ddot{u}_{gR}(t)$, respectively, it can be assumed, that the ground excitation consists of a symmetric component

$$\ddot{u}_{gs}(t) = \frac{\ddot{u}_{gL}(t) + \ddot{u}_{gR}(t)}{2} \tag{33a}$$

and an antisymmetric component

$$\ddot{u}_{ga}(t) = \frac{\ddot{u}_{gL}(t) - \ddot{u}_{gR}(t)}{2} \tag{33b}$$

so that

$$\ddot{u}_{gL}(t) = \ddot{u}_{gs}(t) + \ddot{u}_{ga}(t) \tag{34a}$$

$$\ddot{u}_{gR}(t) = \ddot{u}_{gs}(t) - \ddot{u}_{ga}(t) \tag{34b}$$

In this case

$$p(x, t) = p_{eff}(x, t) = -m\ddot{u}_{gs}(t) - m\ddot{u}_{ga}(t)\left(1 - \frac{2x}{L}\right) \tag{35}$$

can be divided into symmetric and antisymmetric components

$$p_s(x, t) = -m\ddot{u}_{gs}(t) \tag{36a}$$

$$p_a(x, t) = -m\ddot{u}_{ga}(t)\left(1 - \frac{2x}{L}\right) \tag{36b}$$

Substituting Equation (36) into Equations (31) and (32), the generalized modal forces for the considered beam can be expressed as

$$P_s = -\Psi_s\ddot{u}_{gs}(t) \tag{37a}$$

$$P_a = -\Psi_a\ddot{u}_{ga}(t) \tag{37b}$$

where

$$\Psi_s = m \int_0^L \varphi_s(x)\,dx \tag{38}$$

$$\Psi_a = m \int_0^L \varphi_a(x)\left(1 - \frac{2x}{L}\right)dx \tag{39}$$

The possibility of different ground motions at the two supports may exist in some practical situations. However, in most cases, engineers need to consider a simpler case, when both supports are subjected to the same acceleration history, so that $\ddot{u}_{gL}(t) = \ddot{u}_{gR}(t) = \ddot{u}_{gs}(t) = \ddot{u}_g(t)$ and $\ddot{u}_{ga}(t) = 0$. In this case $P_a = 0$, only symmetric modes contribute to the response, and hence, only symmetric modes need to be considered. It should be noted that hereafter, only symmetric support excitation is considered, and some of the expressions derived do not apply to the more general case of multiple support excitation.

EARTHQUAKE RESPONSE SPECTRUM ANALYSIS

Substituting Equations (37a) and (38) into Equation (29), and dividing the latter by M_n, gives the mass normalized modal equation of motion for the considered beam subjected to earthquake excitation (here subscript n is used for the nth mode, although, as noted in the previous section, only symmetric modes are considered)

$$\ddot{z}_n(t) + \omega_n^2 z_n(t) = -\Gamma_n \ddot{u}_g(t) \tag{40}$$

where

$$\Gamma_n = \frac{\Psi_n}{M_n} \tag{41}$$

For classically damped systems, Equation (40) becomes

$$\ddot{z}_n(t) + 2\zeta_n \omega_n \dot{z}_n(t) + \omega_n^2 z_n(t) = -\Gamma_n \ddot{u}_g(t) \tag{42}$$

where ζ_n is the damping ratio for the nth mode. Equation (42) is the same as the equation of motion of an SDOF system, except for the factor Γ_n, so that the peak value of z_n for the nth mode, denoted here by z_{0n}, can be estimated from earthquake response (or design) spectra scaled by Γ_n

$$z_{0n} = \Gamma_n \mathrm{Sd}_n = \Gamma_n \frac{\mathrm{PSa}_n}{\omega_n^2} \tag{43}$$

where Sd_n and PSa_n are the deformation and pseudo-acceleration ordinates, respectively, of a spectrum for damping ratio ζ_n at period $T_n = 2\pi/\omega_n$. The peak displacement $u_{0n}(x)$, the peak equivalent static force $F_{0n}(x)$, the peak bending moment $\mathscr{M}_{0n}(x)$ and the peak shear force $V_{0n}(x)$, at any point along the beam, due to the nth mode, can be calculated using well-known expressions found in textbooks [3] on the dynamics of structures.

The peak values of the total responses can be then estimated by combining the peak modal responses according to one of the common modal combination rules. Because the frequencies of

symmetric modes for the considered beam are usually well separated, the square-root-of-sum-of-squares (SRSS) combination rule is satisfactory. Moreover, in most cases the total responses may be evaluated with sufficient accuracy by taking into account only the contribution of the first mode, and neglecting the contribution of higher modes. As will be illustrated later in the numerical case studies, higher modes have very limited impact on the elastic response of the considered system.

ASSUMED FIRST MODE SHAPE FUNCTIONS

Determination of the generalized modal mass and stiffness requires complex integration of the squared modal shape function and the product of the shape function with its fourth derivative. The 'exact' shape functions of Equations (12) are not convenient for these operations, and approximate functions are used instead. For example, the single-mode spectral method [4] of seismic analysis, adopted by the American Association of State Highway and Transportation Officials (AASHTO), and based on the uniform loading shape, would imply the following first mode shape function for the considered beam:

$$\varphi_1(x) = \frac{3.2(xL^3 - 2x^3L + x^4 + 12BL^4)}{L^4(1 + 38.4B)} \tag{44}$$

Using the function of Equation (49) and well-known structural dynamics equations [3], the dynamic parameters of the first mode can be expressed as

$$M_1 = m\int_0^L [\varphi_1(x)]^2 \, \mathrm{d}x = \frac{(38.4)^2 M}{(1 + 38.4B)^2}\left(B^2 + \frac{B}{30} + \frac{31}{90720}\right) \tag{45}$$

$$K_1 = \mathrm{EI}\int_0^L \varphi_1(x)\,\varphi_1^{\mathrm{iv}}(x) \, \mathrm{d}x = \frac{49.152K_eB}{(1 + 38.4B)^2}(60B + 1) \tag{46}$$

$$\Psi_1 = m\int_0^L \varphi_1(x)\,\mathrm{d}x = \frac{0.64M}{(1 + 38.4B)}(60B + 1) \tag{47}$$

$$\Gamma_1 = \frac{\Psi_1}{M_1} = \frac{(1 + 38.4B)(60B + 1)}{38.4(60B^2 + 2B + 31/1512)} \tag{48}$$

$$M_1^* = \Gamma_1\Psi_1 = \frac{M(60B + 1)^2}{60(60B^2 + 2B + 31/1512)} \tag{49}$$

$$\omega_1^2 = \frac{K_1}{M_1} = \frac{K_eB(60B + 1)}{M(30B^2 + B + 31/3024)} \tag{50}$$

$$T_1 = \frac{2\pi}{\omega_1} = 2\pi\sqrt{\frac{M(30B^2 + B + 31/3024)}{K_eB(60B + 1)}} \tag{51}$$

Alternatively, another first mode shape function, based on a half-sine wave loading shape, can be used

$$\varphi_1(x) = \frac{\sin(\pi x/L) + \pi^3 B}{1 + \pi^3 B} \tag{52}$$

which gives (in a similar manner as before)

$$M_1 = \frac{M(1 + 8\pi^2 B + 2\pi^6 B^2)}{2(1 + \pi^3 B)^2} \tag{53}$$

$$K_1 = \frac{K_e \pi^4 B(1 + 4\pi^2 B)}{2(1 + \pi^3 B)^2} \tag{54}$$

$$\Psi_1 = \frac{M(2 + \pi^4 B)}{\pi(1 + \pi^3 B)} \tag{55}$$

$$\Gamma_1 = \frac{2(2 + \pi^4 B)(1 + \pi^3 B)}{\pi(1 + 8\pi^2 B + 2\pi^6 B^2)} \tag{56}$$

$$M_1^* = \frac{2M(2 + \pi^4 B)^2}{\pi^2(1 + 8\pi^2 B + 2\pi^6 B^2)} \tag{57}$$

$$\omega_1^2 = \frac{K_e \pi^4 B(1 + 4\pi^2 B)}{M(1 + 8\pi^2 B + 2\pi^6 B^2)} \tag{58}$$

$$T_1 = \sqrt{\frac{4M(1 + 8\pi^2 B + 2\pi^6 B^2)}{K_e \pi^2 B(1 + 4\pi^2 B)}} \tag{59}$$

The assumed first mode shape functions of Equations (44) and (52) closely approximate the 'exact' first mode shape function of Equation (12a), which lies (in graphical format) between them. For any positive finite B, Equation (44) produces greater, and Equation (52) produces smaller, than the 'exact' values of first mode shape at any point along the span, except the midspan (where all three functions produce unity). Consequently, the expressions based on the first mode shape of Equation (44) overestimate M_1, K_1, Ψ_1, M_1^*, and underestimate Γ_1. The opposite is true for Equations (53)–(57), which underestimate M_1, K_1, Ψ_1, M_1^*, and overestimate Γ_1. Both Equations (51) and (59) narrowly underestimate the fundamental period T_1.

Equations (45)–(51) and (53)–(59) provide convenient closed form expressions for the first mode dynamic parameters and produce very accurate results, especially Equations (51) and (59) for T_1. The assumed shape function of Equation (44) and the associated expressions for first mode dynamic parameters are more accurate in the range of $B > 0.02$ and become 'exact' when $B = \infty$. Equations (52)–(59) are more accurate in the range of $B < 0.02$ and are 'exact' for $B = 0$. Note, that the assumed shape functions of Equations (44) and (52) at the supports produce more error than any of the associated Equations (45)–(51) and (53)–(59), respectively. Therefore, when evaluating the displacement response at the supports, the use of a shear force expression

$$u_{01}(0) = -\frac{V_{01}(0)}{K_e} = \frac{0.5 M_1^* \omega_1^2}{K_e} \mathrm{Sd}_1 = \frac{\Gamma_1^2 K_1}{2K_e} \mathrm{Sd}_1 \tag{60}$$

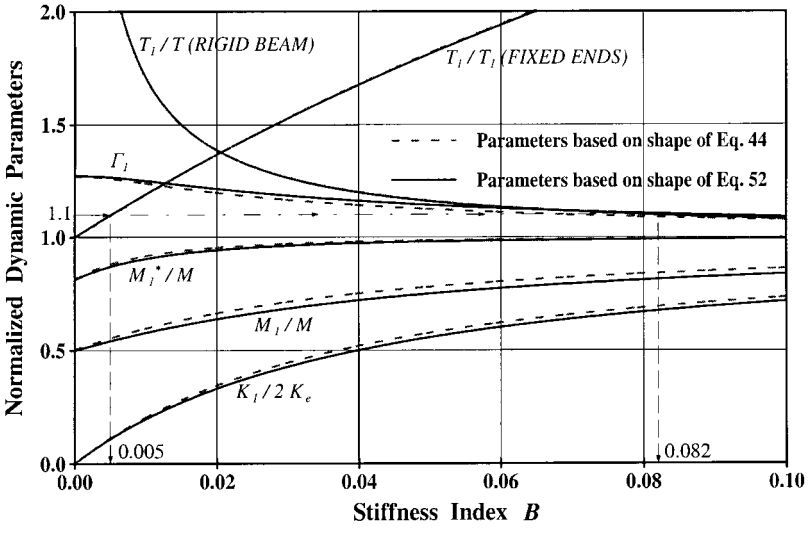

Figure 2. First mode dynamic parameters.

would be more accurate than the direct use of the assumed shape functions. In other words, the expression

$$\varphi_1(0) = \frac{0.5\Psi_1\omega_1^2}{K_e} = \frac{\Gamma_1 K_1}{2K_e} \tag{61}$$

gives improved accuracy for the estimate of the shape function at the support.

EFFECT OF STIFFNESS INDEX B ON THE DYNAMIC PARAMETERS

The variations of the first mode dynamic parameters, depending on the magnitude of the stiffness index B, defined by Equation (9), are illustrated in Figure 2. Γ_1 is non-dimensional, other parameters are given in a normalized form to facilitate comparison with scenarios in which the flexibility of the span or the flexibility of the end conditions is neglected. Each parameter in the figure is represented by two curves: one based on the assumed shape function of Equation (44) (dashed curve), and the other based on the assumed shape function of Equation (52) (solid curve). Note that an 'exact' dynamic parameter curve (except normalized T_1 curves) would lie between the two curves.

It can be observed from Figure 2 that Γ_1 varies between 1.0 and $4/\pi$. The range of M_1^*/M is from $8/\pi^2$ (about 81 per cent) at $B = 0$ to unity (100 per cent) at $B = \infty$. The latter indicates that the first mode becomes more dominant in the dynamic response with increasing index B.

The fundamental period T_1 is shown twice: once normalized by the period of a spring supported infinitely rigid beam (EI $= \infty$)

$$T(\text{RIGID BEAM}) = 2\pi\sqrt{\frac{M}{2K_e}} \tag{62a}$$

and the other time normalized by the fundamental period of a uniform flexible beam with translationally fixed ends ($K_e = \infty$)

$$T_1(\text{FIXED ENDS}) = 2\sqrt{\frac{\text{ML}^3}{\text{EI}\pi^2}} \tag{62b}$$

Neglect of the flexibility of the bridge span or the flexibility of supports leads to artificial stiffening of the system, resulting in shorter fundamental periods. Accurate determination of the fundamental period of bridges is essential in the evaluation of their seismic loading, especially when design spectra exhibit sharp variation of response acceleration coefficient with period. The use of a flat plateau in the short period range of AASHTO spectra [4] shows some wisdom, since 'accurate' periods could be illusory, taking into consideration all the uncertainties associated with material properties and soil conditions. On the other hand, the spectra suggested by the Applied Technology Council (ATC) [5] exhibit sharp peaks in the short period range. The use of such spectra implies a greater degree of accuracy in the assessment of the fundamental period.

The T_1/T (RIGID BEAM) curve, shown in Figure 2, allows the engineer to estimate the error, associated with neglecting the flexibility of the span. For example, for a 10 per cent error tolerance in the estimate of the fundamental period, the assumption of an infinitely rigid span would be justified if B is greater than 0.082. Similarly, the T_1/T_1 (FIXED ENDS) curve represents the elongation in the fundamental period of the actual system over that of the system with assumed infinitely rigid supports. As shown in Figure 2, if the engineer could tolerate no more than a 10 per cent artificial period shortening, the stiffness index B of the system has to be less than 0.005 in order to justify the assumption of translationally fixed span ends.

NUMERICAL EXAMPLES

Three simply supported two-lane highway bridges, shown in Figure 3, are analysed here to illustrate some of the issues raised. Each of the considered bridges has a 200 mm thick, 8 m wide, reinforced concrete deck resting on four steel girders spaced at 2 m (WWF 1200×333 for

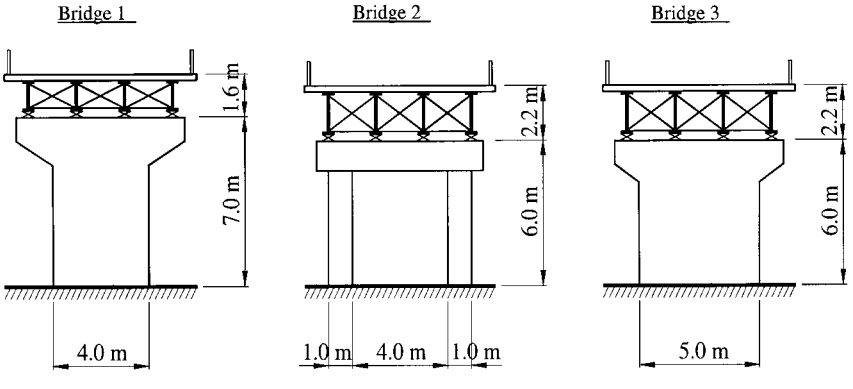

Figure 3. Bridges for numerical examples.

Table I. Numerical examples: dynamic parameters of bridges.

Example	L (m)	M (ton)	EI (N mm^2)	K_e (N/mm)	B ($\times 10^{-2}$)	$K_1/2K_e$	Γ_1	$\varphi_1(0)$	$\Gamma_1 \times \varphi_1(0)$
(1)	(2)	(3)	(4)	(5)	(6)	(7)	(8)	(9)	(10)
Bridge 1	40	286	3.72×10^{17}	147680	3.936	0.497	1.164	0.578	0.673
Bridge 2	70	588	5.02×10^{17}	84410	1.734	0.301	1.225	0.369	0.452
Bridge 3	70	588	5.02×10^{17}	292710	0.500	0.109	1.267	0.138	0.175

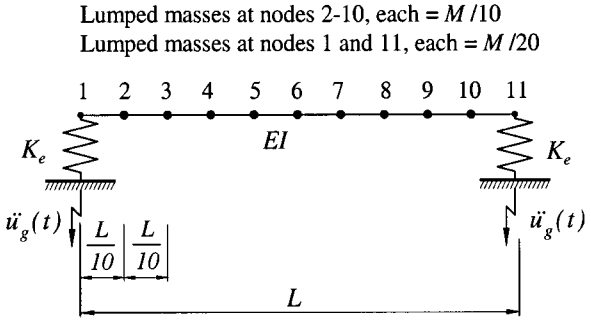

Figure 4. MDOF model for numerical examples.

Bridge 1, and WWF 1800×632 for Bridges 2 and 3). The bridges were modelled as generalized single degree of freedom (SDOF) systems employing the assumed shape function of Equation (52). The dynamic parameters of interest for the three bridges, calculated using Equations (9), (54), (56) and (61), are summarized in Table I.

Each of the three bridges was also modelled as a multiple degree of freedom (MDOF) system, shown in Figure 4. Both modal analysis and elastic time-history analysis of the MDOF model was conducted using the computer program DRAIN-2DX [6]. Mass proportional damping of 5 per cent was used in all time-history simulations. The earthquake acceleration records used for time history analysis are listed in Table II. The values of the spectral deformation Sd (5 per cent damped) for periods of interest, shown in Table II, were computed using the NONSPEC program [7].

The fundamental periods for the three bridges, calculated using various methods discussed above, are compared in Table III. Note that Equations (62a) and (62b), which assume infinitely rigid beam and translationally fixed supports, respectively, produce large errors for all considered bridges. On the other hand, Equation (51) for Bridge 1 and Equation (59) for Bridges 2 and 3 produced very accurate results (in fact, slightly more accurate than the results obtained through the MDOF system modal analysis using DRAIN-2DX, when looking at significant digits beyond the range of adequate engineering accuracy). The 'exact' first mode periods were calculated, using Equation (15), based on $\beta_1 L$ values, determined graphically by plotting Equation (14a). Figure 5 illustrates the plot of frequency equations for Bridge 1 in the range $0 < \beta L < 3\pi$. For this bridge, the 'exact' first four mode shapes (Equation (16)) are shown in Figure 6, and the

Table II. Earthquake acceleration records for analysis.

Event	Date (yy-mm-dd)	Site	Peak acceler. (g)	Duration (s)	*Sd* (mm) for $T =$		
					0.235 s	0.534 s	0.443 s
(1)	(2)	(3)	(4)	(5)	(6)	(7)	(8)
Imperial Valley	40-05-18	El Centro, S00E	0.35	20	11.08	63.76	37.10
Parkfield	66-06-27	Cholame Shandon, Array 2, N65E	0.49	20	9.15	104.11	77.00
San Fernando	71-02-09	Pacoima Dam, S16E	1.17	20	27.14	94.49	104.00
Whittier	87-10-01	Long Beach, Stn. 14242 (chn. 1)	0.24	20	5.87	32.13	17.68
Loma Prieta	89-10-17	Capitola FS, Stn. 47125 (chn. 1)	0.40	20	8.93	48.93	38.86
Cape Mendocino	92-04-25	Petrolia, Stn. 89156 (chn. 3)	0.59	20	11.14	56.20	36.10
Landers	92-06-28	Joshua Tree, Stn. 22170 (chn. 1)	0.28	30	7.86	25.40	21.52
Northridge	94-01-17	Castaic Route, Stn. 24278 (chn. 3)	0.51	15	10.83	82.46	45.18

Table III. Comparison of fundamental periods obtained by various methods.

Method description	Bridge 1 ($\beta_1 L = 2.43143$)		Bridge 2 ($\beta_1 L = 2.73007$)		Bridge 3 ($\beta_1 L = 2.99831$)	
	T_1 (sec)	Error (%)	T_1 (sec)	Error (%)	T_1 (sec)	Error (%)
(1)	(2)	(3)	(4)	(5)	(6)	(7)
Equation (15) (exact solution)	0.23576	NA	0.53434	NA	0.44301	NA
Equation (22) (Maclaurin's series-3 terms)	0.23557	− 0.08	0.53354	− 0.15	0.44228	− 0.16
Equation (23) (Maclaurin's series-2 terms)	0.24456	+ 3.73	0.56013	+ 4.83	0.46463	+ 4.88
Equation (51) (uniform loading shape)	0.23564	− 0.05	0.53346	− 0.16	0.44185	− 0.26
Equation (59) (half-sine-wave loading shape)	0.23523	− 0.22	0.53372	− 0.12	0.44295	− 0.01
Equation (62a) (infinitely rigid beam)	0.19552	− 17.1	0.37081	− 30.6	0.19913	− 55.1
Equation (62b) (translationally fixed ends)	0.14122	− 40.1	0.40352	− 24.5	0.40352	− 8.91
DRAIN-2DX (modal analysis-10 elements)	0.23535	− 0.17	0.53330	− 0.19	0.44250	− 0.12

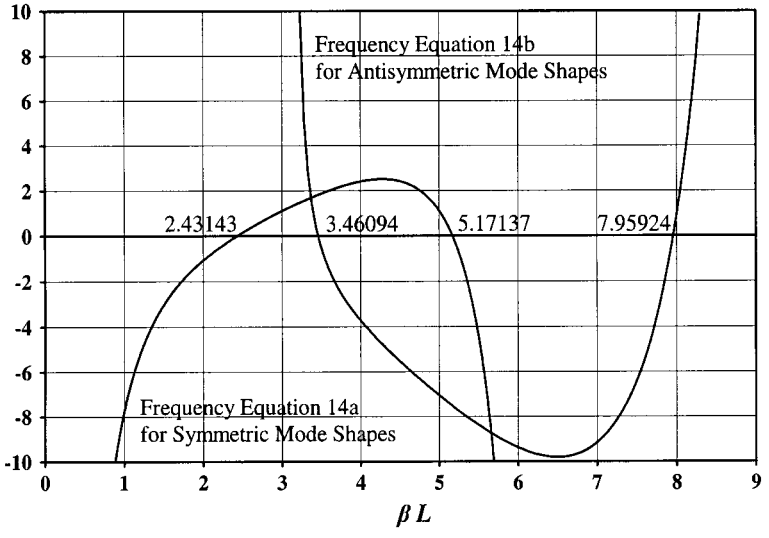

Figure 5. Bridge 1 — plot of frequency equations.

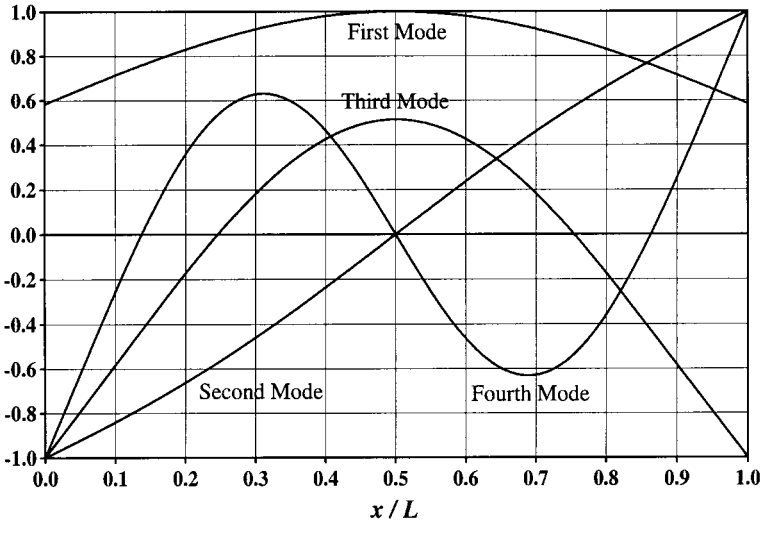

Figure 6. Bridge 1 — exact mode shapes.

approximate first mode shapes functions of Equations (44) and (52) are compared with the 'exact' first mode shape in Figure 7.

Based on the generalized SDOF model used, the predictions of the maximum midspan displacement, $u_0(L/2)$, for each considered ground motion record, were obtained by scaling the respective Sd values from Table II by Γ_1, according to Equation (43). Similarly, using

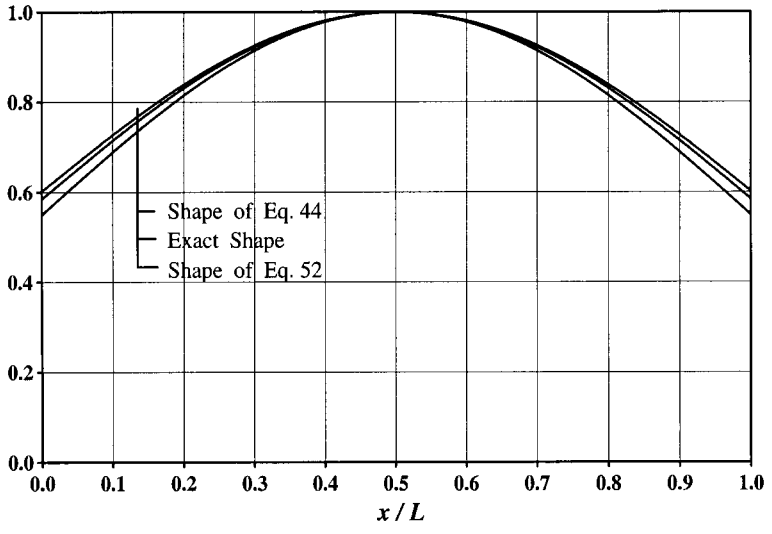

Figure 7. Bridge 1 — first mode shapes.

Table IV. Elastic response based on generalized SDOF model.

Acceleration record	Bridge 1 max. displacements		Bridge 2 max. displacements		Bridge 3 max. displacements	
	$u_0(0)$ (mm)	$u_0(L/2)$ (mm)	$u_0(0)$ (mm)	$u_0(L/2)$ (mm)	$u_0(0)$ (mm)	$u_0(L/2)$ (mm)
(1)	(2)	(3)	(4)	(5)	(6)	(7)
Imperial Valley	7.5	12.9	28.8	78.1	6.5	47.1
Parkfield	6.2	10.7	47.1	127.5	13.5	97.6
San Fernando	18.3	31.6	42.7	115.8	18.2	131.8
Whittier	4.0	6.8	14.5	39.4	3.1	22.4
Loma Prieta	6.0	10.4	22.1	59.9	6.8	49.2
Cape Mendocino	7.5	13.0	25.4	68.8	6.3	45.7
Landers	5.3	9.1	11.5	31.1	3.8	27.3
Northridge	7.3	12.6	37.3	101.0	7.9	57.2

Equation (60), the maximum support displacements, $u_0(0)$, were calculated by scaling the appropriate Sd values by $\Gamma_1 \times \varphi_1(0)$. The results are summarized in Table IV. The maximum midspan (node 6) and support (node 1) displacements, obtained from the results of DRAIN-2DX time history runs, based on the MDOF model, are listed in Table V. By comparing the results presented in Tables IV and V, excellent agreement between the two models can be observed for each bridge in all scenarios.

For completeness, the maximum mid-span displacements, based on the rigid beam SDOF model (with EI $= \infty$) and the fixed ends generalized SDOF model (with $K_e = \infty$), are listed in

Table V
Elastic response based on MDOF model.

Acceleration record	Bridge 1 max. displacements		Bridge 2 max. displacements		Bridge 3 max. displacements	
	Node 1 (mm)	Node 6 (mm)	Node 1 (mm)	Node 6 (mm)	Node 1 (mm)	Node 6 (mm)
(1)	(2)	(3)	(4)	(5)	(6)	(7)
Imperial Valley	7.5	12.8	29.3	77.2	7.1	46.3
Parkfield	6.3	10.5	48.2	125.7	13.8	96.8
San Fernando	18.2	31.2	43.3	116.5	18.1	132.3
Whittier	4.0	6.8	15.4	38.6	3.3	22.1
Loma Prieta	6.0	10.3	21.4	59.7	7.0	49.0
Cape Mendocino	7.5	12.9	26.7	67.4	7.4	45.0
Landers	5.3	9.0	11.8	31.0	4.2	26.8
Northridge	7.5	12.4	37.8	100.4	8.4	56.6

Table VI. Elastic response based on SDOF models that neglect superstructure or support flexibility.

Acceleration record	Bridge 1 maximum mid-span displacement $u_0(L/2)$ (mm)		Bridge 2 maximum mid-span displacement $u_0(L/2)$ (mm)		Bridge 3 maximum mid-span displacement $u_0(L/2)$ (mm)	
	Rigid beam $T = 0.196$ s	Fixed ends $T_1 = 0.141$ s	Rigid beam $T = 0.371$ s	Fixed ends $T_1 = 0.404$ s	Rigid beam $T = 0.199$ s	Fixed ends $T_1 = 0.404$ s
(1)	(2)	(3)	(4)	(5)	(6)	(7)
Imperial Valley	6.2	4.3	23.8	30.6	6.4	30.6
Parkfield	5.1	4.3	47.0	79.7	5.1	79.7
San Fernando	19.2	14.5	94.1	143.0	21.5	143.0
Whittier	4.1	2.9	9.8	15.3	4.0	15.3
Loma Prieta	6.7	6.6	28.9	43.3	7.1	43.3
Cape Mendocino	8.1	4.7	31.0	37.8	8.4	37.8
Landers	4.3	2.5	15.8	20.6	4.5	20.6
Northridge	8.8	5.3	33.0	40.9	9.1	40.9

Table VI. Note, that for the rigid beam model $u_0(0) = u_0(L/2) = \mathrm{Sd}$, and for the Fixed Ends model $u_0(0) = 0$ and $u_0(L/2) = \mathrm{Sd} \times 4/\pi$. As could be expected, the results presented in Table VI do not agree with the results of Table V, based on the MDOF model, because the rigid beam and the fixed ends models do not reflect the considered system appropriately. Furthermore, the error on resulting average displacements by far exceeds the error on the periods reported in Table III. For example, if Bridge 1 was analysed using the common fixed ends model, the calculated mid-span displacement would be underestimated by a factor of 2.4.

The presented numerical case studies show that the generalized SDOF model is sufficiently accurate (at least, when compared to respective MDOF model) for the seismic analysis of symmetric spans of simply supported bridges, even in the lower range of stiffness index B. It means that the time-consuming and error-prone modelling of such bridges as MDOF systems can be avoided. Note, that the lengthy numerical integrations, required by the AASHTO single mode spectral analysis method procedure, can also be avoided through the use of the efficient closed-form expressions for the first mode dynamic parameters, derived in this paper.

CONCLUSIONS

The interaction of superstructure and support flexibilities in the dynamic response of simply supported bridges to transverse ground motion was investigated using a formal analytical approach and some simplified procedures. It was found, that the span/support stiffness index completely defines the modal shapes. The effects of this index on the first mode dynamic parameters of the system were discussed. Two sets of closed-form expressions (based on two different assumed shape functions), useful for hand calculations, were derived for the dynamic parameters of the generalized SDOF model. The accuracy of the derived equations was assessed, and their use in predicting elastic response of bridges was demonstrated in numerical examples. It was shown that the generalized SDOF model produces accurate results for symmetric spans of simply supported bridges, and that the contribution of the higher modes to the seismic response is of little significance in those cases.

The parametric study presented in this paper quantifies the errors made when assumptions of rigid superstructure or rigid supports are adopted in the seismic analysis of simply supported bridges. Neglect of superstructure or support flexibility leads to an artificial stiffening of a bridge system, resulting in a shorter estimated fundamental period, which in turn may result in a significant error in the evaluation of seismic loads, especially when design spectra exhibit sharp variations of spectral acceleration with period. The presented curves for normalized fundamental periods facilitate quick assessment of the error involved and allow practising engineers to identify the instances where such an error becomes of significance.

ACKNOWLEDGEMENTS

The Natural Sciences and Engineering Research Council of Canada is acknowledged for its financial support through a Collaborative Grant on Innovative Seismic Retrofit of Existing Bridges. The Ontario Graduate Scholarship of the first author from the Ontario Ministry of Education and Training is gratefully acknowledged. The authors also express their appreciation of the Internet site of the California Strong Motion Instrumentation Program (http://www.consrv.ca.gov/dmg/csmip/index.html), from which most of the acceleration records for numerical examples were downloaded.

REFERENCES

1. Zahrai SM, Bruneau M. Energy dissipating stiff diaphragms for steel bridges in seismic regions. *Journal of Constructional Steel Research*, Paper No. 034, 1998; **46**(1–3): 42–43. (Abstract on pp. 42–43, full paper on the CD-ROM that accompanied Vol. **46** issues 1–3.)
2. Sarraf M, Bruneau M. Ductile seismic retrofit of steel deck—truss bridges—design applications. ASCE *Journal of Structural Engineering* 1998; **124**: 1263–1271.

3. Chopra AK. *Dynamics of Structures*: *Theory and Applications to Earthquake Engineering*. Prentice-Hall: Englewood Cliffs, NJ, 1995.
4. *Standard Specifications for Highway Bridges* (16th edn). American Association of State Highway and Transportation Officials: Washington, DC, 1996.
5. *Improved Seismic Design Criteria for California Bridges: Provisional Recommendations. Report No. ATC-32*, Applied Technology Council, Redwood City, CA, June 1996.
6. Prakash V, Powell GH, Campbell S. DRAIN-2DX: Base Program Description and User Guide: Version 1.10′, *Report No. UCB/SEMM-93/17*, University of California, Berkeley, CA, November 1993.
7. Mahin S, Lin J. Construction of inelastic response spectra for single-degree-of-freedom systems: computer program and applications. *Report No. UCB/EERC-83/17*, Earthquake Engineering Research Center, University of California, Berkeley, CA, June 1983.

